



A photochemical proposal for the preparation of ZnAl_2O_4 and MgAl_2O_4 thin films from β -diketonate complex precursors



G. Cabello^{a,*}, L. Lillo^a, C. Caro^a, M. Seguel^a, C. Sandoval^a, G.E. Bueno-Core^b, B. Chornik^c, M. Flores^c

^a Departamento de Ciencias Básicas, Facultad de Ciencias, Universidad del Bío-Bío, Chillán, Chile

^b Instituto de Química, Pontificia Universidad Católica de Valparaíso, Valparaíso, Chile

^c Departamento de Física, Facultad de Ciencias Físicas y Matemáticas, Universidad de Chile, Santiago 8370415, Chile

ARTICLE INFO

Article history:

Received 4 October 2015

Received in revised form 17 January 2016

Accepted 23 January 2016

Available online 24 January 2016

Keywords:

Inorganic compounds

Oxides

Thin films

Chemical synthesis

Photoelectron spectroscopy

ABSTRACT

ZnAl_2O_4 and MgAl_2O_4 thin films were grown on Si(100) and quartz plate substrates using a photochemical method in the solid phase with thin films of β -diketonate complexes as the precursors. The films were deposited by spin-coating and subsequently photolyzed at room temperature using 254 nm UV light. The photolysis of these films results in the deposition of metal oxide thin films and fragmentation of the ligands from the coordination sphere of the complexes. The obtained samples were post-annealed at different temperatures (350–1100 °C) for 2 h and characterized by FT-Infrared spectroscopy, X-ray diffraction (XRD), X-ray photoelectron spectroscopy (XPS), atomic force microscopy (AFM), and UV–vis spectroscopy. The results indicate the formation of spinel-type structures and other phases. These characteristics determined the quality of the films, which were obtained from the photodeposition of ternary metal oxides.

© 2016 Elsevier Ltd. All rights reserved.

1. Introduction

Spinel-type oxides AB_2O_4 , where A and B stand for divalent and trivalent metal cations, respectively, have a wide range of applications as ceramic, catalyst, magnetic, and host materials because of their good thermal and chemical stabilities [1,2]. In the spinel structure, the oxygen ions form a cubic close-packed (ccp) structure, and the A and B cations occupy two different crystallographic sites – tetrahedral and octahedral holes in the ccp structure – that provide different local symmetries for different ions. Therefore, spinels may take different forms, such as (a) normal spinel, where the A and B cations are distributed in the tetrahedral and octahedral sites, respectively; (b) inverse spinel, where the A cations are in the octahedral sites, and half of the B cations are pushed to the tetrahedral sites; and (c) mixed spinel, where both A and B cations are randomly distributed in both sites [2]. Studies of the cation distribution in spinels have attracted much attention because they enable a better understanding of the correlations between the structure and the properties such as color, magnetic behavior, catalytic activity, optical properties, etc.,

which strongly depend on the occupation of these two sites by the metals.

In this context, ternary metal oxides such as ZnAl_2O_4 and MgAl_2O_4 have been widely investigated in the vast array of useful applications. Various preparation methods have been used to synthesize oxide spinels, such as the sol–gel method [3,4], solid-state reaction [5,6], hydrothermal reaction [7,8] and combustion process [9,10]. The development of alternative methods or modifications of existing methodologies is the subject of permanent concern for a large range of mixed-metal oxides to search for an efficient route by which to obtain high purity, homogeneity, single phases and small and uniform particle sizes of these materials.

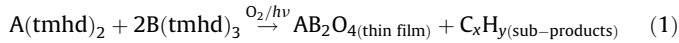
The photochemical synthesis of ceramic materials with light irradiation (both ultraviolet and visible) is an alternative method for obtaining new and unique structured inorganic compounds and semiconductor materials [11]. Photochemical synthesis is different from other synthesis methods because it is selective. This selectivity occurs because the light absorption features of the reactants determine their reaction products.

The species generated by photon excitation or photolysis can be the primary species of the final products or precursors that subsequently react to form new species and the final products [11]. In this study, we propose the application of a photochemical method to synthesize ZnAl_2O_4 and MgAl_2O_4 thin films. This

* Corresponding author. Fax: +56 42 2463046.

E-mail addresses: gerardocabelloguzman@hotmail.com, gcabello@ubiobio.cl (G. Cabello).

method consists of the direct irradiation of β -diketonate complexes on substrates that are not affected by the UV light. The development of this method requires that the precursor complexes form stable amorphous thin films after spin coating onto a suitable substrate, and the photolysis of these films result in the photo-extrusion of the ligands to leave thin films of metals or metal oxides on the surface, depending on the reaction conditions:



where: A = Zn or Mg, B = Al, and $\text{tmhd} = (\text{CH}_3)_3\text{C}-\text{CO}-\text{CH}-\text{CO}-\text{C}-(\text{CH}_3)_3$.

2. Experimental

2.1. Preparation of amorphous thin films (where A = Zn or Mg)

The precursor complexes $\text{Al}(\text{tmhd})_3$, $\text{Zn}(\text{tmhd})_2$ and $\text{Mg}(\text{tmhd})_2$ were purchased from Aldrich Chemical Company. The substrates for the film deposition were quartz plates ($2 \times 2 \text{ cm}^2$) and n- and p-type silicon (100) wafers ($1 \times 1 \text{ cm}^2$), which were obtained from Wafer World Inc., Florida, USA.

The $\text{A}(\text{tmhd})_2$ and $\text{Al}(\text{tmhd})_3$ complexes were homogenized and mixed in a molar proportion of 1:2 in CH_2Cl_2 or ethanol solution. The thin films were prepared as follows. A silicon chip was placed on a spin coater and rotated at a speed of 600 rpm. A portion (0.5 mL) of a solution of both precursor complexes in CH_2Cl_2 was dispensed onto the silicon chip and allowed to spread. The motor was stopped after 30 s, and a thin film of the complex remained on the chip. The quality of the films was examined using optical microscopy ($500\times$ magnification).

2.2. Photolysis of complexes as films on Si(100) surfaces

All photolysis experiments were performed following the identical procedure. First, the FT-IR spectrum of the starting film was obtained. Then, the chip was placed under a UV-lamp setup, which was equipped with two 254 nm 6W tubes, in air. The reaction progress was monitored by determining the FT-IR spectra at different time intervals, following the decrease in IR absorption of the complexes. After the FT-IR spectrum showed no evidence of the starting material, the chip was rinsed several times with dry acetone to remove all remaining organic products on the surface

prior to the analysis. To obtain films of a specific thickness, successive layers of the precursors were deposited by spin-coating and irradiated as previously described. This process was repeated several times until the desired thickness was achieved. Post-annealing was performed under a continuous flow of synthetic air at different temperatures (350–1100 °C) for 2 h in a programmable Lindberg tube furnace. The schematic sequence of the photochemical deposition method to synthesize ternary metal oxides is shown in Fig. 1.

2.3. Characterization of the thin films

The FT-IR spectra were obtained with a 4 cm^{-1} resolution in a PerkinElmer Spectrum Two FT-IR spectrophotometer. The UV spectra were obtained with 1 nm resolution in a PerkinElmer Model Lambda 25 UV-vis spectrophotometer. X-ray diffraction (XRD) patterns were obtained using a D8 Advance Bruker X-ray diffractometer; the X-ray source was Cu 40 kV/30 mA. A semi-quantitative phase composition is calculated from the peak intensities for different phases in the sample.

X-ray photoelectron spectra (XPS) were recorded on an XPS-Auger PerkinElmer electron spectrometer Model PHI 1257, which included an ultra-high vacuum chamber, a hemispherical electron energy analyzer and an X-ray source that provided unfiltered $K\alpha$ radiation from its Al anode ($h\nu = 1486.6 \text{ eV}$). The pressure of the main spectrometer chamber during data acquisition was maintained at ca. 10^{-7} Pa . The binding energy (BE) scale was calibrated using the peak of adventitious carbon, which was set to 284.6 eV. The accuracy of the BE scale was $\pm 0.1 \text{ eV}$. The surface morphology of the samples was examined using atomic force microscopy (AFM) in an AFM/STM Omicron Nanotechnology model SPM1 in contact mode.

3. Results and discussion

3.1. Photochemistry of the precursor complexes

The photoreactivity of some Al(III) and Zn(II) β -diketonate complexes was reported in other articles as the precursors in the photodeposition of Al_2O_3 [12,13] and ZnO [14,15] thin films, respectively. In this work, we proposed the use of Al(III), Zn(II) and Mg(II) 2,2,6,6-tetramethyl-heptanedionate (tmhd) complexes as precursors to evaluate their photoreactivity and further

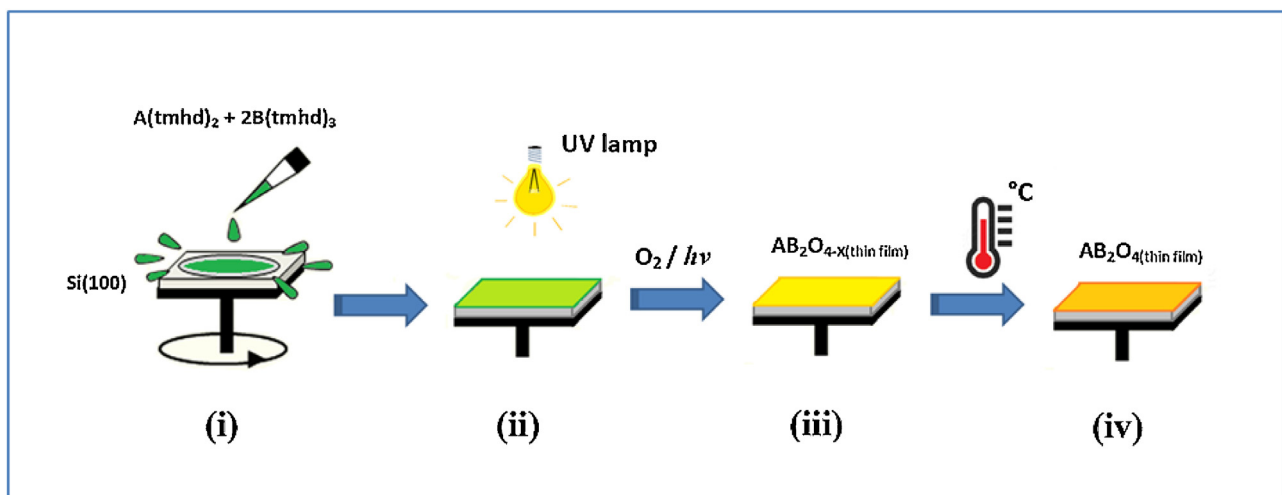


Fig. 1. Schematic sequence of the photo-deposition process: (i) deposition of precursor complexes by spin-coating; (ii) photo-reactivity of the precursor complexes under a UV lamps set; (iii) photo-deposition of ternary metal oxides in air (as-deposited); and (iv) post-annealing of the photo-deposited films.

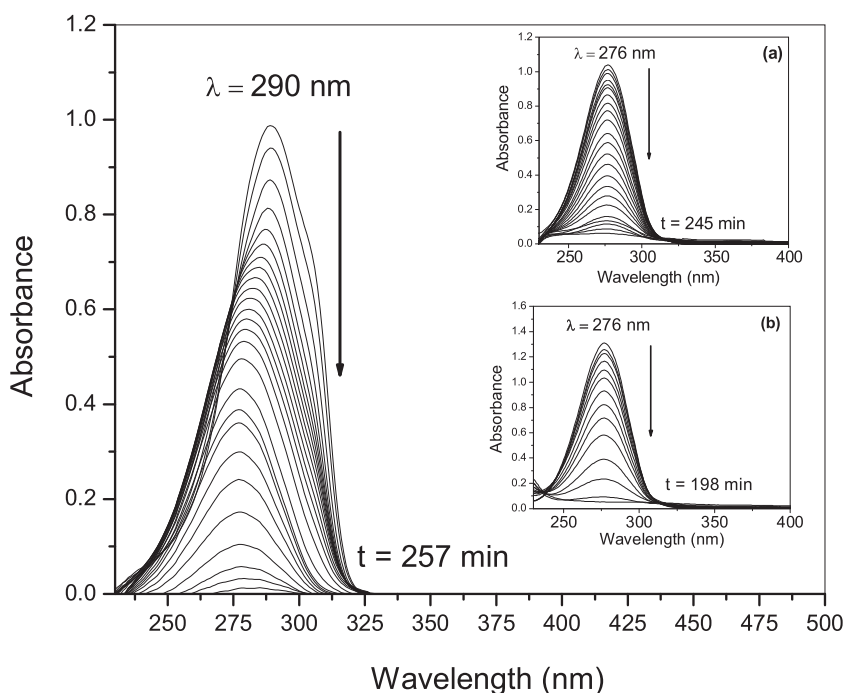


Fig. 2. Changes in the UV spectrum of a solution in CH_2Cl_2 of $\text{Al}(\text{tmhd})_3$ complex (2.50×10^{-4} mol/L) upon 257 min irradiation. Insets: (a) $\text{Zn}(\text{tmhd})_2$ complex (3.47×10^{-6} mol/L) after 245 min of irradiation, (b) $\text{Mg}(\text{tmhd})_2$ complex (2.34×10^{-5} mol/L) after 198 min of irradiation with 254 nm light.

photodeposition as mixed-metal oxides. When the dichloro-methane-diluted solutions of these complexes ($\leq 10^{-4}$ mol/L) were photolyzed with 254 nm UV light, a gradual decrease in the absorption bands of these complexes was observed after few minutes of irradiation. Fig. 2 shows the UV profile for the photoreaction of these complexes, which was obtained by determining the UV spectra of the samples at different time intervals. In all cases, the spectra exhibit a single band at 290 or 276 nm, which was assigned to a π - π^* ligand electronic transition of a carbonyl group ($\text{C}=\text{O}$). These spectral changes, which consist of a gradual decrease in the absorption bands, demonstrate that these β -diketonate complexes are susceptible to their structural photo-fragmentation and photo-reduction of the metallic species. Similar results were observed in other studies [16,17].

To investigate the solid-state photochemistry, films of the mixed-metal precursor complexes in a molar proportion of 1:2 of $\text{M}(\text{tmhd})_2$ and $\text{Al}(\text{tmhd})_3$ (where $\text{M} = \text{Zn}$ or Mg) were deposited on Si wafers by spin-coating and irradiated in air with a 254 nm UV source. The irradiation at 24, 48 and 72 h of these films in air led to a decrease in absorption, which is associated with the ligands, as shown by the FT-IR monitoring of the reaction. At time zero (t_0), Fig. 3 shows the vibration modes that correspond to the 2,2,6,6-tetramethylheptanedione ligand at 2963, 1589 and 1096 cm^{-1} , which is assigned to the $\text{C}-\text{H}$, $\text{C}=\text{O}$ and $\text{C}-\text{O}$ groups, respectively. At the end of the photolysis, after a 72 h irradiation period, minimum absorptions are observed in the infrared spectrum. These absorptions correspond to sub-products from the photo-degradation of the diketonate complexes on the surface,

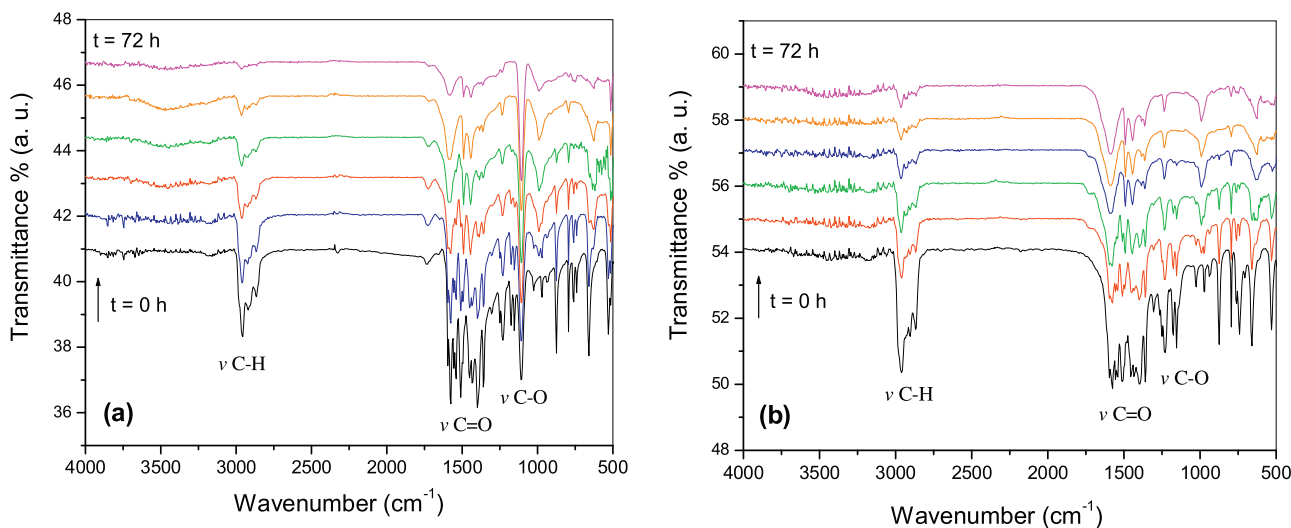


Fig. 3. Changes in the FT-IR spectra of the films after 24, 48 and 72 h of irradiation with 254 nm light of (a) $\text{Zn}(\text{tmhd})_2$ and $\text{Al}(\text{tmhd})_3$ and (b) $\text{Mg}(\text{tmhd})_2$ and $\text{Al}(\text{tmhd})_3$ complexes in a molar proportion of 1:2.

which are partially removed by washing with dry acetone or ethanol.

3.2. Characterization of the ZnAl_2O_4 and MgAl_2O_4 thin films

FT-IR spectroscopy was used to characterize preliminary the as-deposited films and films that were annealed at 350 °C, 650 °C, 950 °C and 1100 °C. According to some studies [3,8], the spinel displays stretching bands in the 500–900 cm^{-1} range, which are associated with the vibrations of metal–oxygen, aluminum–oxygen and metal–oxygen–aluminum bonds. Fig. 4 compares the infrared spectra curves of the annealed samples of ZnAl_2O_4 and MgAl_2O_4 films. This comparison shows that the samples that were annealed at 350 and 650 °C exhibit some characteristic bands. The band at $\sim 3400 \text{ cm}^{-1}$ corresponds to the presence of OH groups, which are attributed to the adsorption of water on the surface of the film. Another band at $\sim 1100 \text{ cm}^{-1}$ is associated to the stretching vibrations of C–O species, which were generated as sub-products from the precursor complexes, and another broad band at $\sim 810 \text{ cm}^{-1}$ which can be attributed to the vibrational modes of different groups corresponding to M–O and M–O–M (M = Zn, Mg or Al) [18–20], which formed gradually during the heat treatment.

On the other hand, the samples that were annealed at 950 and 1100 °C exhibit some characteristic bands in the range of 400–900 cm^{-1} . Fig. 4a shows the FT-IR spectra of the ZnAl_2O_4 films, whose bands appear at (1) 484, (2) 550, (3) 658 and (4) 890 cm^{-1} . These bands correspond to the regular spinel structure and are ascribed to the Zn–O and Al–O vibrations of the tetrahedral [ZnO_4] and octahedral [AlO_6] groups [8]. However, the spectra of the MgAl_2O_4 films (Fig. 4b) exhibit bands at (1) 515, (2) 692 and (3) 870 cm^{-1} , which are associated with the lattice vibrations of tetra- and octahedrally coordinated metal ions [21]. However, these results only indicate that there is an interaction of oxygen with metal ions and it is not possible to confirm the formation of a spinel-type structures.

XRD was used to study the crystalline structure of the samples annealed at 950 and 1100 °C. The XRD pattern of ZnAl_2O_4 (Fig. 5a) show peaks at 2θ (°) = 31.2, 36.8, 44.8, 49.1, 55.7 and 59.4, which can be indexed as the (2 2 0), (3 1 1), (4 0 0), (3 1 1), (4 2 2) and (5 1 1) diffraction planes, respectively. The intensities and positions of these peaks are consistent with those of reference JCPDS Card No. 05-0669. Similar results were observed by other authors [3,8,19]. However, for the ZnAl_2O_4 films that were annealed at 950 °C, the

peaks corresponding to the ZnO formation were observed. Many of these signals are not observed when the samples were annealed at 1100 °C, which shows an initiation of spinel phase and low crystallinity at 950 °C. However, with the increase in temperature to 1100 °C, the crystallinity of the ZnAl_2O_4 spinel products increased.

Thus, the XRD results show that after the thermal treatment at 950 °C of the photodeposited films, different phases are formed with a partial formation of the spinel. The effects of annealing at higher temperatures (≥ 1000 °C) may promote the formation of a pure spinel phase without secondary phases, as observed in the spinel synthesis using other methods [22,23]. We have determined that ZnAl_2O_4 films that are annealed at 950 °C are mainly composed of two phases, which were estimated at 71.4 and 28.6% w/w of ZnAl_2O_4 and ZnO, respectively, whereas the films annealed at 1100 °C are composed of 80.3% of ZnAl_2O_4 and 19.7% w/w of ZnO.

However, Fig. 5b shows the XRD patterns of the MgAl_2O_4 samples at 950 and 1100 °C. The diffraction data of the films are consistent with the reference JCPDS Card No. 01-072-6944, which indicates that these films are spinel phases with a cubic structure [24]. The main reflections of the samples annealed at 950 °C are observed at 2θ (°) = 18.9, 31.2, 36.8, 44.8 and 59.4, which are associated with the (1 1 1), (2 2 0), (3 1 1), (4 0 0) and (5 1 1) crystal planes of MgAl_2O_4 , and there are other peaks of intermediate products such as corundum (Al_2O_3) and periclase (MgO). Therefore, our samples consist of a mixture of spinel (26.6% w/w), MgO (60.4% w/w) and Al_2O_3 (13.1% w/w). In addition, a temperature of 950 °C was not sufficient to produce a pure crystalline product. With an increase in annealing temperature to 1100 °C, the diffraction peaks of the spinel become sharper because of the increase in crystallinity of the spinel phase, but some impurities remain: spinel (50.1% w/w), MgO (20.8% w/w) and Al_2O_3 (29.1%). Studies on the preparation of mixed oxides (MgO– Al_2O_3) [25,26] have shown that there is a strong interaction between the alumina lattice and magnesium metal to form MgAl_2O_4 spinel-type. The formation of Mg(II)–Al(III) solid solution of the spinel type increase by increasing of calcination temperature, and that could explain the drastic decrease in the % w/w of MgO from 950 to 1100 °C.

Moreover, some studies [27] have found the incorporation of magnesium into the Al_2O_3 lattice. The addition of MgO stabilizes the Al_2O_3 phase because the Mg ions preferentially substitute for tetrahedrally coordinated Al^{3+} in the Al_2O_3 lattice [28].

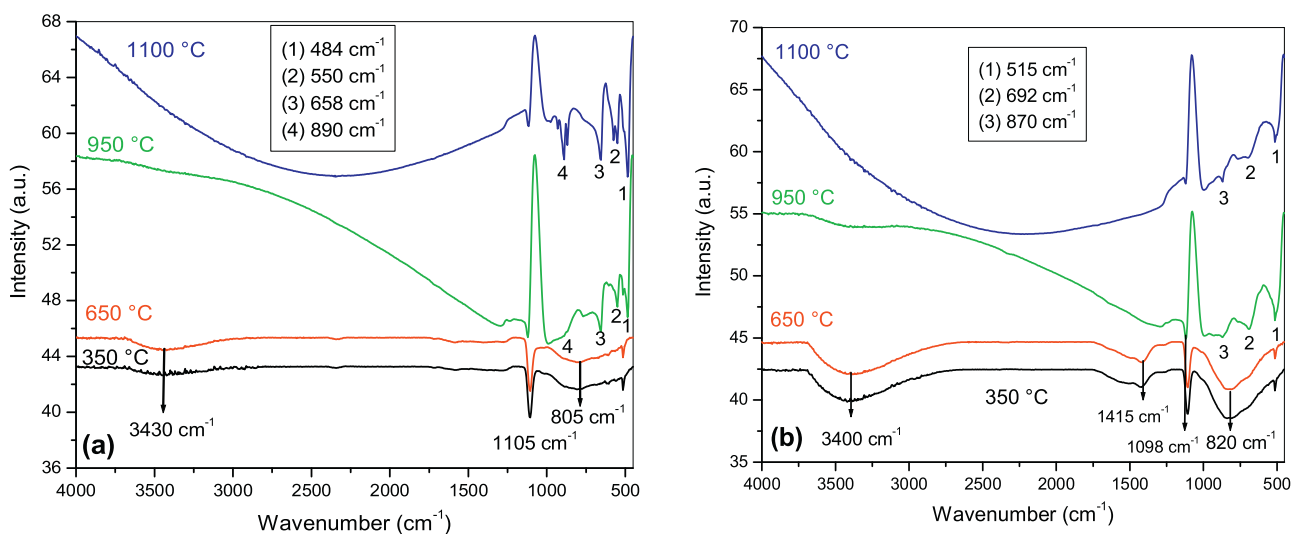


Fig. 4. FT-IR spectra of (a) ZnAl_2O_4 and (b) MgAl_2O_4 thin films that were photo-deposited and annealed at 350, 650, 950 and 1100 °C.

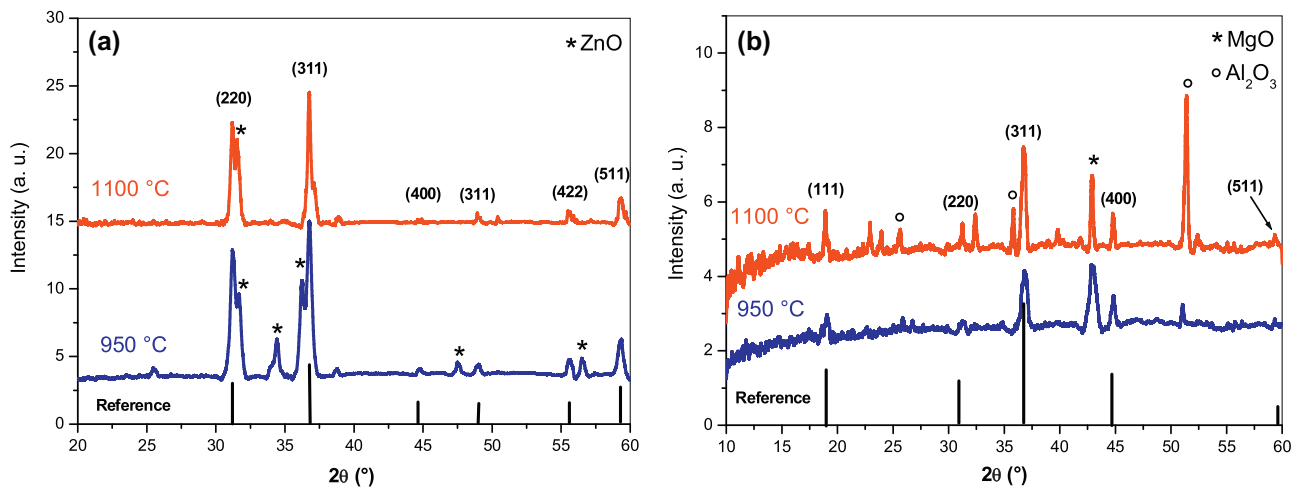


Fig. 5. XRD pattern of the samples, which were photo-deposited and annealed at 950 and 1100 °C for 2 h. (a) ZnAl_2O_4 and (b) MgAl_2O_4 .

In this case, the results show that the MgAl_2O_4 spinel phase develops with increasing annealing temperature but also suggest that the complex $\text{Mg}(\text{tmhd})_2$ is not a suitable precursor to use with $\text{Al}(\text{tmhd})_3$ in this photochemical methodology to deposit ternary metal oxides as MgAl_2O_4 . The nature of the precursor complexes plays a decisive role in the efficient deposition of mixed metal oxides. The differences in solubility and compatibility of both complexes determine the quality of the resulting films [29]. Other authors have reported [30] that the use of high concentrations of each precursor in the spinel synthesis can cause the formation of secondary phases, and the change in $[\text{A}]/[\text{B}]$ ratio in the precursor solutions decides the stoichiometric composition of the AB_2O_4 films.

The elemental composition of the samples was further determined using XPS. The XPS survey spectrum (Fig. 6a) indicates that the prepared ZnAl_2O_4 sample consists of Zn, Al, O and C elements. Fig. 6b shows the high-resolution XPS spectra of Zn $2p_{3/2}$, which are fitted with two peaks at 1024.1 eV (5.4%) and 1022.5 eV (94.6%). These peaks at approximately 1024 and 1022 eV are assigned to octahedral and tetrahedral Zn^{2+} ions, respectively [1].

In Fig. 7a, the O 1s peak is fitted with two components centered at 532.6 (18.9%) and 531.2 eV (81.1%). The higher-energy peak corresponds to O–H bonds from absorbed water molecules because of the environmental moisture [31], whereas the

lower-energy peak is attributed to metal–oxygen bonds [32]. The high-resolution spectrum of Al 2p (Fig. 7b) appears as a broad and asymmetric band at 74.1 eV, which indicates that Al^{3+} ions have more than one coordination environment [1]. Thus, some authors have reported [31,32] that the Al 2p signal can be adjusted by two peaks at 75.6 and 74.2 eV and assigned to Al^{3+} ions in the octahedral (VI) and tetrahedral (IV) sites, respectively.

The XPS study was also applied to the MgAl_2O_4 samples. The XPS survey spectrum in Fig. 8a confirms the presence of Mg, Al, O and C. High-resolution XPS spectra of Mg 2s and Mg 2p at 88.9 and 50.1 eV, respectively, are shown in Fig. 8b. These values are similar to those observed for the other spinel [33,34]. The O 1s line (Fig. 9a) consists of two peaks at 531.1 (35%) and 531.7 eV (65%). The signal at 531.7 eV is reported to come from O sites of the spinel lattice [32], and the signal at 531.1 eV possibly comes from AlO_x (Al in the AlO_4 tetrahedral site or AlO_6 octahedral site). The signal that is typically located at ~ 532 eV and tentatively ascribed to chemisorbed O or hydroxyl species was not observed here.

A high-resolution spectrum of the Al 2p peak, which is shown in Fig. 9b, is fitted with two Gaussian–Lorentzian curves at 74.1 (93.4%) and 78.9 eV (6.6%). The peak at the lower binding energy can be ascribed to the Al^{3+} ions at the tetrahedral sites, whereas the peak at higher binding energy can be assigned to the Al^{3+} ions that occupy the octahedral sites. The binding energy values of the two

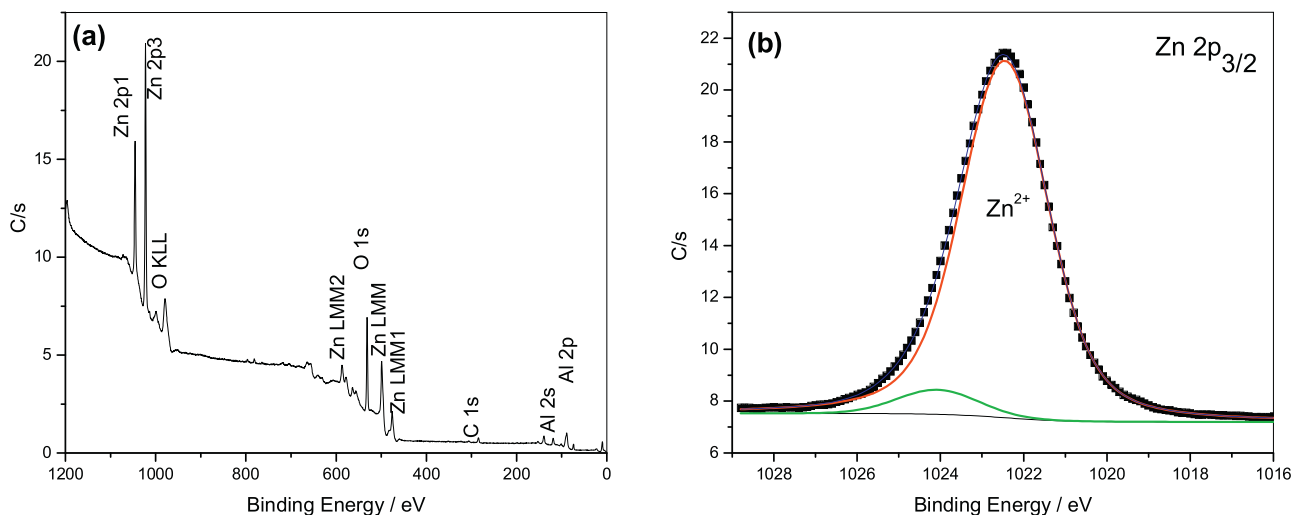


Fig. 6. XPS survey spectrum of the ZnAl_2O_4 thin films, which were annealed in air at 1100 °C for 2 h. (a) Full XPS spectra and (b) Zn $2p_{3/2}$ spectra.

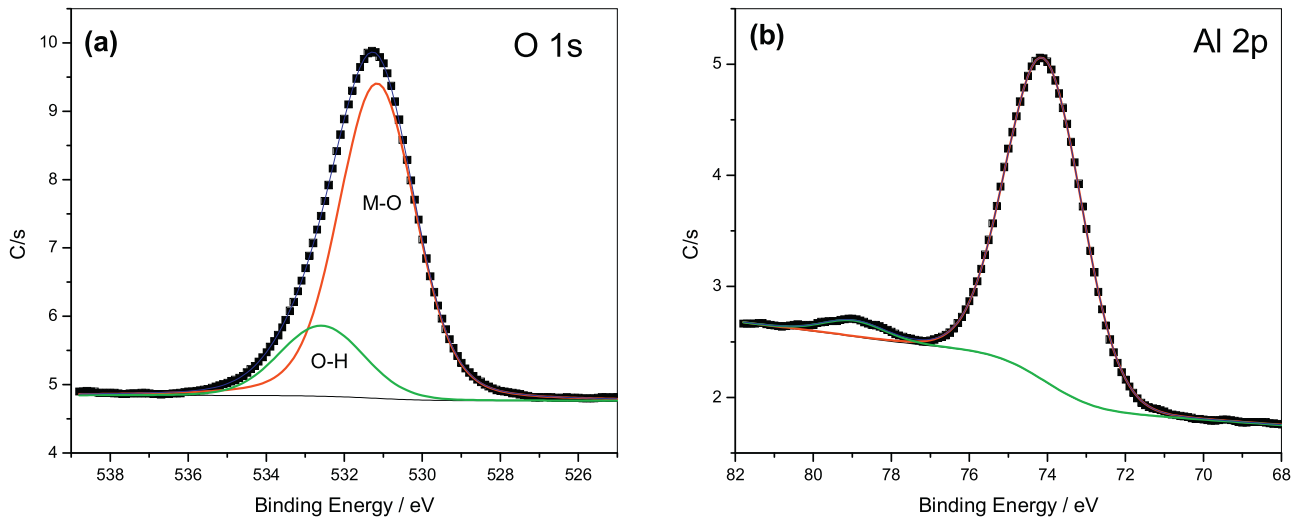


Fig. 7. High-resolution XPS spectrum of the ZnAl_2O_4 thin films, which were annealed in air at 1100°C for 2 h. (a) O 1s and (b) Al 2p spectra.

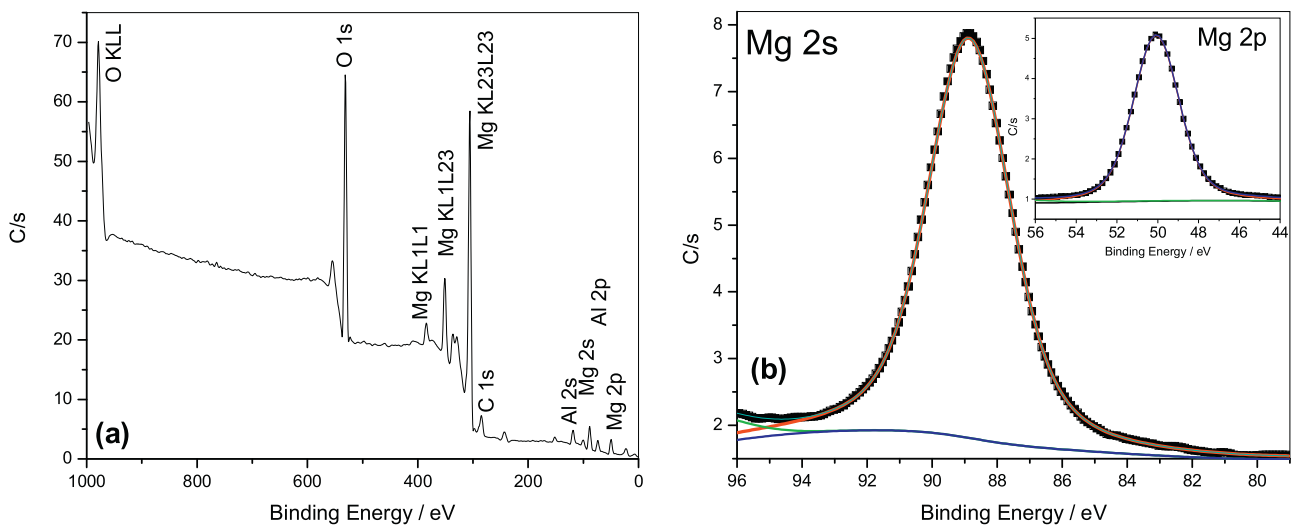


Fig. 8. (a) XPS survey spectra of the MgAl_2O_4 thin films, which were annealed in air at 1100°C for 2 h. (b) Mg 2s spectra. Inset: Mg 2p spectra.

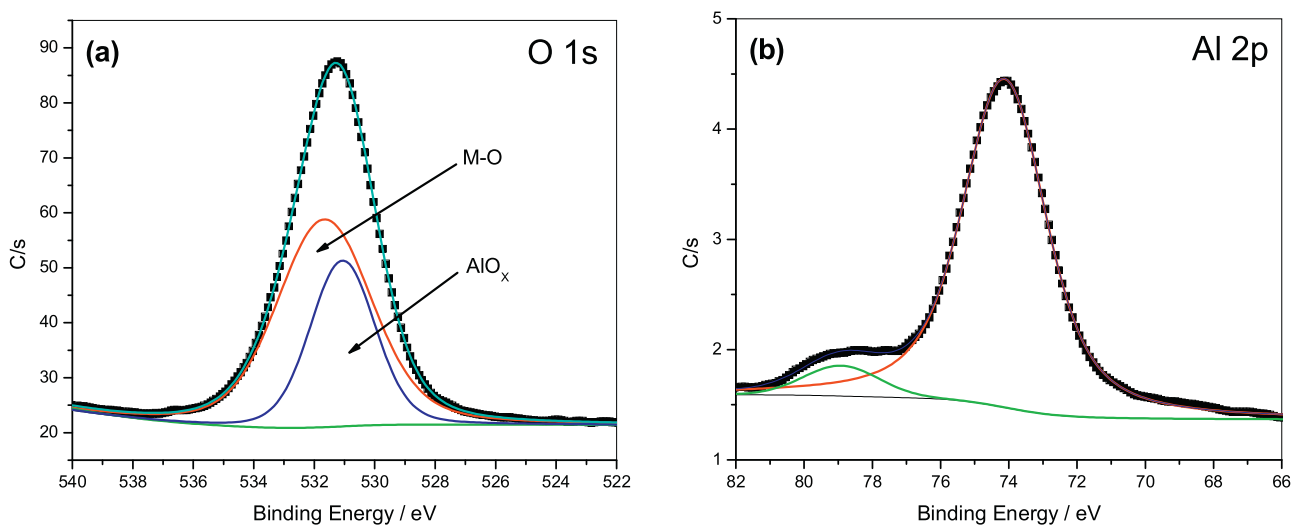


Fig. 9. Narrow-scan XPS spectrum of the MgAl_2O_4 thin films, which were annealed in air at 1100°C for 2 h. (a) O 1s and (b) Al 2p spectra.

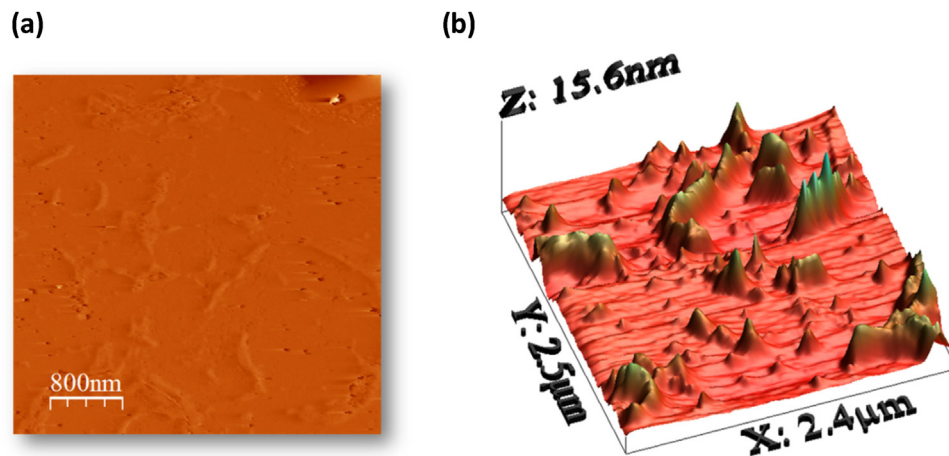


Fig. 10. AFM micrographs of ZnAl₂O₄ films: (a) two-dimensional image and (b) three-dimensional image.

peaks are consistent with those reported for Al³⁺ ions in other materials [1,31].

3.3. Morphology observation

The surface morphology of the samples was observed using AFM. The 2D image of ZnAl₂O₄ films (Fig. 10a) shows that the samples that were photodeposited and annealed at 1100 °C have a smooth surface morphology, and there is no evidence of a granular structure. A careful examination of the 3D image (Fig. 10b) shows that the film surface is non-uniform.

The surface roughness can be quantitatively identified by the root-mean-squared roughness (RMS, roughness: R_{rms}). R_{rms} is given by the standard deviation of data from AFM images, and determined using the standard definition as follows:

$$R_{\text{rms}} = \sqrt{\frac{\sum_{n=1}^N (Z_n - \bar{Z})^2}{N - 1}} \quad (2)$$

where Z_n represents the height of the n th data, Z is equal to the mean height of Z_n in AFM topography, and N is the number of the data [35,36]. In this statistic evaluation the studied surface was equal to $2.5 \times 2.3 \mu\text{m}$ in area. (See Fig. 10). The AFM image showed that the RMS roughness of the ZnAl₂O₄ thin films was 1.50 nm, which implies that the prepared films are relatively smooth. As described in [35], this characteristic significantly affects the optical

losses. Because the film has a small surface roughness, there is a decrease in optical losses through scattering, which leads to high transparency quality in the films.

On the other hand, in Fig. 11 shows the AFM micrographs of MgAl₂O₄ films, which were photodeposited and annealed at 1100 °C. In both images, an irregular surface is observed as in previous samples. The examined surface was equal to $2.5 \times 2.4 \mu\text{m}$ in area RMS roughness determined was 2.75 nm. The surface morphology is commonly highly dependent on the crystallinity and purity of the thin films; therefore, they are important factors for controlling the surface roughness of the films. The surface heterogeneity of our films can be explained by the formation of other phases, which were identified in the XRD analysis, during the deposition process, which creates a difficult homogeneous morphology in the generation of the spinel. The use of separate precursors to grow spinel-type ternary metal oxides sometimes results in some deviations from stoichiometry in the films, which leads to point defects and surface irregularities [37].

3.4. Optical properties

The UV–vis transmission spectra of both samples in the wavelength range of 200–900 nm are shown in Fig. 12. Both films show identical profiles with a strong and gradual absorption below 400 nm. The MgAl₂O₄ films have a higher absorption band

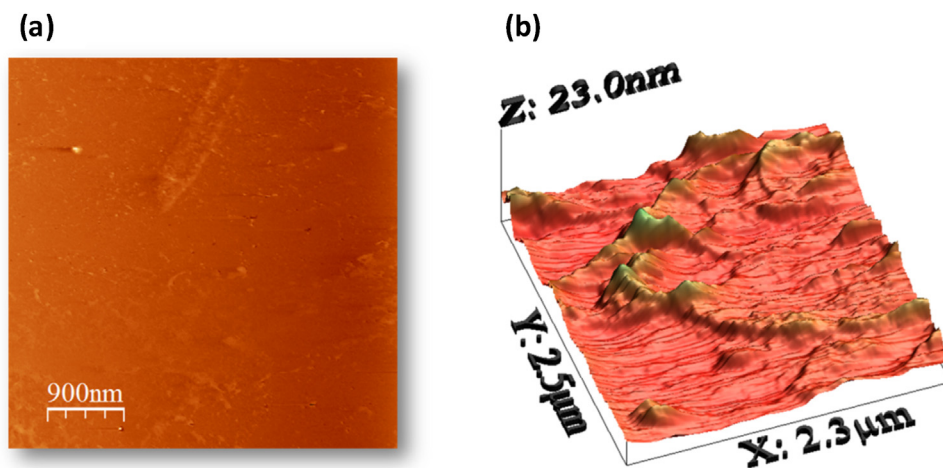


Fig. 11. AFM micrographs of MgAl₂O₄ films: (a) two-dimensional and (b) three-dimensional images.

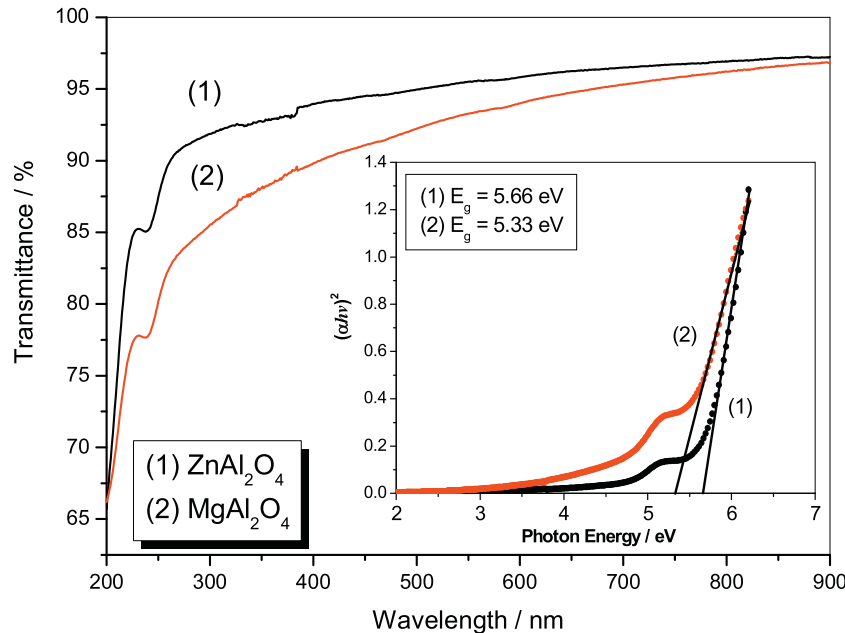


Fig. 12. Transmittance spectra of (1) zinc aluminate and (2) magnesium aluminate thin films. Inset: square of the absorption coefficient as a function of the photon energy to determine the optical band gap (E_g) of the samples.

probably because of some defect structures in the formation of secondary phases (MgO and Al_2O_3). We also observe an increasing in roughness, as clearly identified in our XRD and AFM analysis. For the direct transition, the optical band gap energy (E_g) of these samples was determined using the following equation:

$$(\alpha hv)^2 = B(hv - E_g) \quad (3)$$

where E_g is the optical band gap, hv is the incident photon energy, and B is a constant. The band gap of the films was calculated using Tauc's plot by plotting $(\alpha hv)^2$ vs. hv as shown in the inset of Fig. 11 and extrapolating the linear portion of the absorption edge to find the intercept with the energy axis. The determined E_g value for the MgAl_2O_4 was 5.3 ± 0.2 eV, which is closer to the values reported by other researchers, such as 6.2 eV [22], 5.85 eV [9], and 4.1–4.6 eV [38].

However, the band gaps of ZnAl_2O_4 samples are found at 5.6 ± 0.2 eV, which is notably different from other studies, such as 4.0–4.5 eV [39], 3.47–3.54 eV [40] 3.8–3.9 eV [41]. These measured band gaps depend on the material and its characteristics such as crystallinity and stoichiometry.

4. Conclusions

A simple photochemical deposition method was explored to prepare ZnAl_2O_4 and MgAl_2O_4 thin films. Zn(II) , Mg(II) and Al(III) β -diketonate complexes were proposed as the precursors for the photodeposition of spinel-type ternary metal oxides. Annealing the films at 950°C led to the partial formation of the spinel; however, when the films were annealed at 1100°C , the development and crystallinity of the spinel are favored. The prepared sample was characterized using different tools: FT-IR, XRD, XPS, AFM and UV-vis. The results of these studies reveal the chemical composition of AB_2O_4 and the generation of intermediate products such as ZnO , MgO and Al_2O_3 . Nevertheless, further studies are necessary to better control the structure and morphology of the ZnAl_2O_4 and MgAl_2O_4 thin films and to enhance the understanding of the film formation mechanism. The use of single-source precursors to prepare ZnAl_2O_4 and MgAl_2O_4 films can be an

alternative for controlling the composition and growth of the spinel at lower temperatures [42].

Acknowledgment

The authors are grateful for the financial support of FONDECYT (National Fund for Scientific and Technological Development), Chile, Grant No. 1130114.

References

- [1] Xiulan Duan, Duorong Yuan, Fapeng Xu, *Inorg. Chem.* 50 (2011) 5460–5467.
- [2] V. Sreeja, T.S. Smitha, Deepak Nand, T.G. Ajithkumar, P.A. Joy, *J. Phys. Chem. C* 112 (2008) 14737–14744.
- [3] A.G. Khaledi, S. Afshar, H.S. Jahromi, *Mater. Chem. Phys.* 135 (2012) 855–862.
- [4] M. Kumar, M. Mohapatra, V. Natarajan, *J. Lumin.* 149 (2014) 118–124.
- [5] Sonia Pin, Marco Suardelli, Francesco D. Acapito, Giorgio Spinolo, Michele Zema, Serena Tarantino, Luisa Barba, Paolo Ghigna, *J. Phys. Chem. C* 117 (2013) 6113–6119.
- [6] D. Mohapatra, D. Sarka, *J. Mater. Process. Technol.* 189 (2007) 279–283.
- [7] Chao Ma, Xiang Ying Chen, Shi Ping Bao, *Micro Meso. Mater.* 129 (2010) 37–41.
- [8] Zhengru Zhu, Qidong Zhao, Xinyong Li, Yonghua Li, Caizhi Sun, Ge Zhang, Yongqiang Cao, *Chem. Eng. J.* 203 (2012) 43–51.
- [9] W.A.I. Tabaza, H.C. Swart, R.E. Kroon, *Physica B* 439 (2014) 109–114.
- [10] Shu Fen Wang, Feng Gu, Meng Kai Lu, Xiu Feng Cheng, Wen Guo Zou, Guang Jun Zhou, Shu Mei Wang, Yuan Yuan Zhou, *J. Alloys Compd.* 394 (2005) 255–258.
- [11] Xinsheng Liu, *Inorganic photochemical synthesis, Modern Inorganic Synthetic Chemistry*, (2011), pp. 29–150 (Chapter 6).
- [12] W.L. Law, Ross H. Hill, *Thin Solid Films* 375 (2000) 42–45.
- [13] M.D. Hudson, C. Trundle, C.J. Brierley, *J. Mater. Res.* 6 (1988) 1151–1157.
- [14] G.E. Buono-Core, G. Cabello, A.H. Klahn, R. Del Río, R.H. Hill, *J. Non-Cryst. Solids* 352 (2006) 4088–4092.
- [15] G.E. Buono-Core, A.H. Klahn, G. Cabello, L. Lillo, *Polyhedron* 62 (2013) 1–6.
- [16] S. Giuffrida, G.G. Condorelli, L.L. Costanzo, G. Ventimiglia, R. Lo Nigro, M. Favazza, E. Votrico, C. Bongiorno, I.L. Fragala, *J. Nanopart. Res.* 9 (2007) 611–619.
- [17] S. Scire, S. Giuffrida, C. Crisafulli, P.M. Riccobene, A. Pistone, *J. Nanopart. Res.* 13 (2011) 3217–3228.
- [18] X. Song, S. Zheng, J. Zhang, W. Li, Q. Chen, B. Cao, *Mater. Res. Bull.* 47 (2012) 4305–4310.
- [19] F.M. Stringhini, E.L. Foletto, D. Sallet, D.A. Bertuol, O. Chivavone-Filho, C.A. Oller do Nascimento, *J. Alloys Compd.* 588 (2014) 305–309.
- [20] M.A. Subhan, T. Ahmed, P. Sarker, T.T. Pakkanen, M. Suvanto, M. Horimoto, H. Nakata, *J. Lumin.* 148 (2014) 98–102.
- [21] S. Tripathy, D. Bhattacharya, *J. Asian Ceram. Soc.* 1 (2013) 328–332.
- [22] I.V. Beketov, A.I. Medvedev, O.M. Samatov, A.V. Spirina, K.I. Shabanova, *J. Alloys Compd.* 586 (2014) S472–S475.

- [23] H. Jiang, Z. Cao, R. Yang, L. Yuan, H. Xiao, J. Dong, *Thin Solid Films* 539 (2013) 81–87.
- [24] Fa-tang Li, Ye Zhao, Ying Liu, Y.-J. Hao, R.-H. Liu, D.-S. Zhao, *Chem. Eng. J.* 173 (2011) 750–759.
- [25] M. Abdollahifar, M., Haghighi, Ali A. Babaluo, S. K. Talkhoncheg, *Ultrason Sonochem.*, <http://dx.doi.org/10.1016/j.ultsonch.2015.12.010>.
- [26] M. Abdollahifar, M. Haghighi, Ali A. Babaluo, *J. Ind. Eng. Chem.* 20 (2014) 1845–1850.
- [27] J.A. Wang, A. Morales, X. Bokhimi, O. Novaro, T. Lopez, R. Gomez, *Chem. Mater.* 11 (1999) 308–313.
- [28] T.R. Hinklin, R.M. Laine, *Chem. Mater.* 20 (2008) 553–558.
- [29] C.E. Knapp, L.D. Prassides, S. Sathasivam, I.P. Parkin, C.J. Carmalt, *ChemPlusChem* 79 (2014) 122–127.
- [30] T. Oshima, M. Niwa, A. Mukai, T. Nagami, T. Suyama, A. Ohtomo, *J. Cryst. Growth* 386 (2014) 190–193.
- [31] K.G. Tshabalala, S.-H. Cho, J.-K. Park, S.S. Pitale, I.M. Nagpure, R.E. Kroon, H.C. Swart, O.M. Ntwaeaborwa, *J. Alloys. Compd.* 509 (2011) 10115–10120.
- [32] S.S. Pitale, V. Kumar, I.M. Nagpure, O.M. Ntwaeaborwa, H.C. Swart, *Appl. Surf. Sci.* 257 (2011) 3298–3306.
- [33] A. Villa, A. Gaiassi, I. Rossetti, C.L. Bianchi, K. Benthem, G.M. Veith, L. Prati, *J. Catal.* 275 (2010) 108–116.
- [34] S. Wu, J. Xue, R. Wang, J. Li, *J. Alloys. Compd.* 585 (2014) 542–548.
- [35] R. Ashiri, Ali Nemati, M.S. Ghamasari, H. Aadelkhani, *J. Non-Cryst. Solids* 355 (2009) 2480–2484.
- [36] Y. Leprince-Wang, K. Yu-Zhang, *Surf. Coat. Technol.* 140 (2001) 155–160.
- [37] J.-H. Boo, S.-B. Lee, S.-J. Ku, W. Koh, C. Kim, K.-S. Yu, Y. Kim, *Appl. Surf. Sci.* 169–170 (2001) 581–586.
- [38] M.Y. Nassar, I.S. Ahmed, I. Samir, *Spectrochim. Acta Part A* 131 (2014) 329–334.
- [39] R.T. Kumar, N.C.S. Selvam, C. Ragupathi, L.J. Kennedy, J.J. Vijaya, *Powder Technol.* 224 (2012) 147–154.
- [40] T. Wei, Y. Zhang, Ye Yang, R. Tan, P. Cui, W. Song, *Surf. Coat. Technol.* 221 (2013) 201–206.
- [41] C. Peng, G. Li, D. Geng, M. Shang, Z. Hou, J. Lin, *Mater. Res. Bull.* 47 (2012) 3592–3599.
- [42] S. Mathur, M. Veith, T. Ruegamer, E. Hemmer, H. Shen, *Chem. Mater.* 16 (2004) 1304–1312.